

Evaluating the Activation Barriers for Transition Metal N₂O Reactions

Annelies Delabie, Chris Vinckier, Michaela Flock, and Kristine Pierloot*

Chemistry Departement, University of Leuven, Celestijnenlaan 200F, 3001 Heverlee-Leuven, Belgium

Received: December 31, 2000; In Final Form: March 19, 2001

The reactions of 3d transition metal atoms with N₂O, producing the metal oxide and N₂, have been studied by means of density functional theory and the coupled cluster method CCSD(T). The importance of charge transfer in the reaction mechanism has been investigated. For Sc, Ti, and V, the transition state is very reagent-like, and almost no charge transfer occurs. On the other hand, charge transfer from the metal 4s orbital into the N₂O LUMO becomes more important when moving to the right in the 3d series. The reactions with Sc, Ti, and V proceed almost without energy barriers, whereas for Mn, Fe barriers around 9 kcal/mol are calculated. For transition metal atoms with a 3dⁿ4s² ground-state configuration, a correlation is found between the activation barriers and the binding energy of the formed metal oxide. The 3dⁿ⁺¹4s¹ configuration gives rise to a higher reactivity than the 3dⁿ4s² configuration.

1. Introduction

Oxidation reactions between transition metal atoms and N₂O, producing the metal oxide and N₂, are quite exothermic because of the high binding energy of the metal oxides and the low binding energy of oxygen in N₂O. Despite the high exothermicity, most of these reactions are inefficient even at room temperature, indicating the presence of activation barriers.^{1–3} Different reaction mechanisms have been proposed to account for the kinetics of 3d transition metal–N₂O reactions.

The inefficiency of the Ti–N₂O reaction was first explained by means of the oxygen abstraction model.² In this model, a neutral oxygen atom is transferred to the metal to form the metal oxide product. Transition metal atoms (except for Cr and Cu) are characterized by a 3dⁿ4s² configuration, whereas their oxides have 3dⁿ⁺¹4s¹ configurations. The crossing between the 3dⁿ4s² and 3dⁿ⁺¹4s¹ potential energy surfaces is then responsible for the energy barrier. No such barriers are expected to be encountered for transition metals in the 3dⁿ⁺¹4s¹ state, which explains the increased reactivity of the excited-state atoms. However, the oxygen abstraction model also implies that the height of the energy barrier is correlated with the metal excitation energy to the lowest 3dⁿ⁺¹4s¹ configuration, thus predicting the wrong order for the magnitude of the rate constants of Sc, Ti, V.⁴

A second model proposed for the reaction mechanism of metal–N₂O reactions is the electron-transfer process.^{4–6} During the reaction, an electron transfer occurs from the metal atom to the N₂O LUMO, resulting in the bending of the N₂O system and a weakening of the N–O bond. According to this model, the activation barrier should vary with the ionization potential of the metal. This could indeed explain the observed trend for the rate constants $k(\text{Sc}) > k(\text{V}) > k(\text{Ti})$.

For the reactions of N₂O with alkali metals, alkaline earth metals and transition metals Fontijn observed a correlation between the experimental activation barriers and the sum of the metal ionization energy and s–p promotion energy of the metal.^{7–9} He explained this by means of a semiempirical model

based on resonance theory, where the activated complex is assumed to be composed of resonance interactions between covalent and ionic structures. The main resonance structure is characterized by a covalent interaction between oxygen and the metal s-orbital. Mixing with excited states (which have metal p-character) in the activated complex lowers the activation barrier because the orbital overlap increases and possibly lessens electron exchange repulsion between metal atom and N₂O. The addition of ionic character (resulting from the interaction between N₂O[−] and M⁺) further lowers the energy barrier.

However, when rate constants for the reactions of Mn and Fe with N₂O were experimentally determined, it became clear that the resonance interaction model does not accurately describe the energy barriers of these reactions.^{10,11} The observed discrepancy was ascribed to both the neglect of the specific d-electron configuration and the electronic structure of the product metal oxide in the model. It has also been suggested in studies on oxidation reactions of W and Mo that the electronic configurations of 3d and 4s electrons should be considered.^{6,12} Furthermore, Campbell found that for reactions of N₂O with transition metal atoms, there is no correlation between the activation energy and the other parameters such as ionization potential, s–p or s–d promotion energy, the metal oxide bond energy or the exothermicity of the reaction.¹⁰

Only one ab initio study on the reaction mechanism of transition metal ions with N₂O has so far been reported: the reactions of N₂O with Sc, Ti and V were treated with density functional theory (DFT) using the BP86 functional.¹³ No transition state structures were found, implying that the energy barrier for these reactions should be very low (within 3–5 kcal/mol), in agreement with experiment. However, the calculations indicate that electron transfer from the metal atoms to N₂O is an essential element of the reaction mechanism, which is in contradiction with the findings of Campbell.¹⁰

This work presents an ab initio study of the reaction of the transition metal atoms of the entire first row with N₂O. Our objective was to identify trends in the reactivity across the 3d series. N₂O is one of the greenhouse gases and is also involved in the depletion of stratospheric ozone. Emission reduction of N₂O can be achieved by using heterogeneous catalysts for the

* To whom correspondence should be addressed. E-mail: Kristine.Pierloot@chem.kuleuven.ac.be

TABLE 1: Geometric Parameters (Distances in Å, Angles in Degrees) for Transition Structures M–O–N₁–N₂ Obtained at the B3LYP/TZVP Level^a

	M–O	O–N ₁	N ₁ –N ₂	M–O–N ₁	N ₂ –N ₁ –O
Sc(² A')	2.312 (0.42)	1.214 (1.64)	1.116 (2.94)	126.3	171.9
Ti(³ A')	2.251 (0.43)	1.212 (1.63)	1.116 (2.94)	120.9	175.7
V(⁴ A')	2.266 (0.39)	1.217 (1.64)	1.123 (2.95)	124.0	168.0
Cr(⁷ A')	2.242 (0.39)	1.230 (1.63)	1.134 (2.97)	128.7	160.3
Mn(⁶ A')	2.315 (0.40)	1.250 (1.56)	1.140 (2.90)	104.1	148.5
Fe(⁵ A')	2.083 (0.50)	1.263 (1.55)	1.137 (2.95)	115.9	150.0
Co(⁴ A')	2.026 (0.59)	1.267 (1.46)	1.138 (2.69)	117.2	150.2
Ni(³ A')	1.956 (0.67)	1.282 (1.45)	1.143 (2.63)	117.4	145.9
Ni(³ A')	1.961 (0.67)	1.278 (1.45)	1.143 (2.63)	117.3	146.6
Cu(² A')	1.854 (0.89)	1.499 (1.12)	1.141 (2.71)	112.3	125.4
free N ₂ O		1.185 (1.76)	1.123 (2.96)		180.0

^a Bader covalent bond orders are shown between brackets.

decomposition or reduction of N₂O, often containing transition metal atoms or ions.^{14,15} In combustion systems, metal atoms can be introduced directly in the combustion process to reduce the N₂O emission in exhausts.¹⁶ Furthermore, N₂O has been proposed as an intermediate in decomposition and reduction of NO_x by Cu- and Co-catalysts.¹⁷ Fundamental insight in the reactivity of transition metal atoms with N₂O will contribute to the understanding and optimization of possible application systems.

2. Computational Details

Geometry optimizations were performed based on density functional theory (DFT) using the B3LYP functional. The triple- ζ basis sets of Ahlrichs (TZV),¹⁸ augmented with a p-polarization function, were used. The unrestricted formalism has been employed for the open-shell systems. The stationary points were characterized by vibrational analysis at the same level. Also, the ZPE (zero-point vibrational energy) was calculated at this level. The transition state structures all represent saddlepoints, characterized by one negative eigenvalue of the Hessian matrix. The intrinsic reaction coordinate (IRC) was then calculated, starting from the transition state structure in the direction of both reagents and products, to probe the reaction path and check if the correct transition state was located. Atomic charges and spin densities were provided both by Mulliken population analysis and by Bader analysis.¹⁹ The Mulliken orbital populations were also checked. In the Bader analysis, covalent bond orders were also calculated.²⁰ All these calculations were performed using the GAUSSIAN 98 package.²¹

UMPT(2) (Unrestricted second-order Möller–Plesset perturbation theory) and UCCSD (unrestricted coupled cluster) geometry optimizations of the transition state structure [CuONN][‡] were also performed, to check the quality of the B3LYP structure. The same basis sets as in the B3LYP calculations were used (TZV(P)). All electrons were considered in the correlation treatments. These calculations were performed by means of the ACESII code.²²

To accurately evaluate the activation barrier, we performed coupled cluster single point calculations using the B3LYP structures. These CCSD(T) calculations were performed using the MOLCAS-4.1 program.²³ To be able to describe the 3p–3d intershell correlation effects,²⁴ new ANO (Atomic Natural Orbitals) basis sets for the transition metals were constructed. The starting primitive basis sets were (21s15p10d6f4g). To construct the ANOs, exactly the same procedure was used as described by Pou–Amerigo et al.,²⁵ with the exception that now also the 3s and 3p electrons were included in the correlation treatment. These basis sets were made in collaboration with B. J. Persson.²⁶ The number of contracted functions used in the

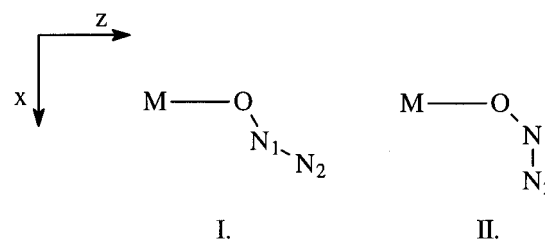


Figure 1. Structure of the transition state for Sc and Ti (I.) and for V–Cu (II.).

CCSD(T) calculations was [7s6p5d2f1g]. For N and O, we used a (14s9p4d3f) primitive set, contracted to [4s3p2d], from the ANO-L molcas basis set library.²⁷ The CCSD(T) reference wave function was obtained by performing a ROHF (restricted open shell Hartree–Fock) calculation. In the CCSD(T) calculations, the metal 3s, 3p, 3d, and N, O, 2s, and 2p electrons were considered in the correlation treatment. Finally, scalar relativistic corrections (Darwin and mass–velocity term) have been added to the CCSD(T) energies. They were obtained at the ROHF level using first-order perturbation theory. We note here that the relativistic effect on the activation barriers never exceeded 0.6 kcal/mol, except in the case of Ni, which will be further discussed.

It was found that the transition metal atoms and N₂O can form an encounter complex before moving to the transition state. These M–N₂O complexes are however very weak. The activation barrier of the M–N₂O reaction was therefore calculated as the difference in energy between the transition state structure and the initial reagents (the transition metal and N₂O). For Sc no encounter complex could be located. Only complexation with the oxygen side of N₂O was considered.

3. Results and Discussion

3.1 Transition State Structures. Structural parameters of the transition state structures (TS) are collected in Table 1. All transition state structures are planar (C_s symmetry). N₂O is bound with its oxygen side to the metal, and the N₂O system is bent. There is a marked difference in the structure of the transition state of both Sc and Ti compared to the other transition metals (V–Cu). The two types of structure are shown in Figure 1. For Sc and Ti, the central nitrogen of N₂O points toward the metal (structure I), while in the case of V–Cu, this nitrogen is bent outward, away from the metal (structure II). The N–N bond is slightly shorter in structure I compared to free N₂O, whereas a weakening is observed for the other metals (structure II). In the experimental studies of the Ni–N₂O reaction, it was found that the two lowest lying Ni states (4s²3d⁸ (³F₄) and 4s¹3d⁹ (³D₃)) are both reactive.²⁸ The transition states on the

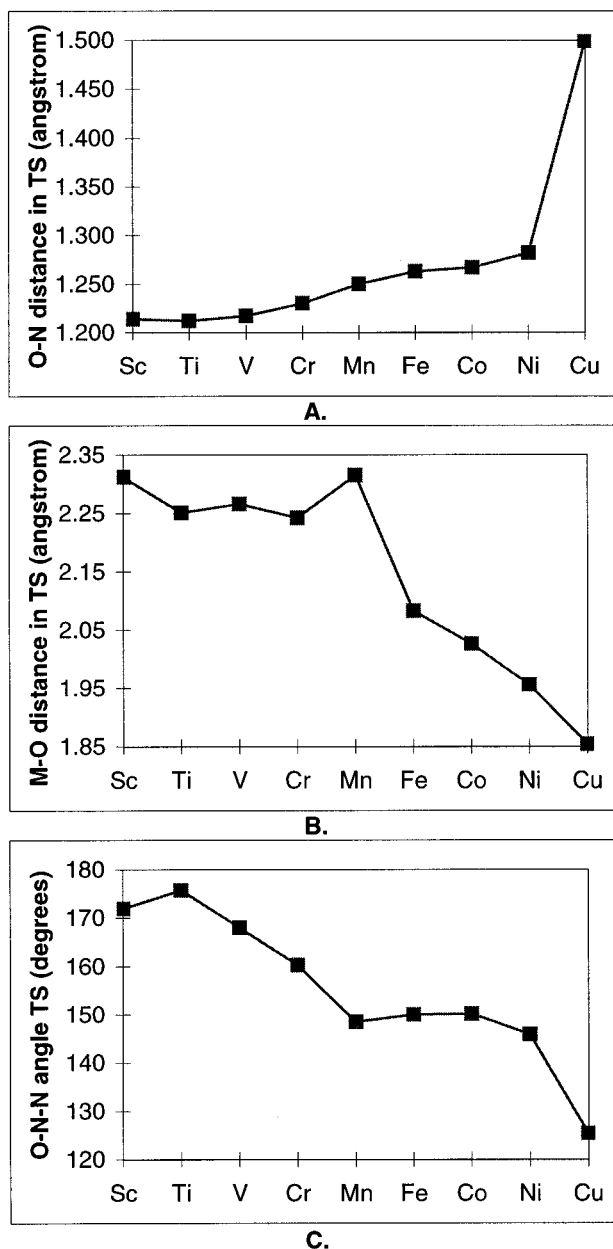


Figure 2. Trends across the 3d series for geometric parameters of the transition state structure [MON₁N₂][‡]. (A) O-N₁ distance (at the B3LYP/TZV(P) level) as a function of Z; (B) M-O distance (at the B3LYP/TZV(P) level) as a function of Z; and (C) N₂-N₁-O angle (at the B3LYP/TZV(P) level) as a function of Z.

two surfaces were calculated, they belong to different symmetry representations. The ³A' structure is characterized by a 4s¹3d⁹ configuration, whereas the ³A'' structure is the transition state on the 4s²3d⁸ surface. The two structures and energies are however very similar.

According to the Hammond postulate, the transition states of exothermic reactions resemble the reagents. Indeed, as one can see from Table 1, the O-N₁ covalent bond order in the transition state structures is not that much smaller than the value observed in the free N₂O molecule (1.76). In Figure 2, the trend in M-O and O-N₁ distances across the 3d series is shown. Graph 2.A clearly shows that the O-N₁ bond distance enlarges when moving to the right through the 3d row, conform with the decrease of the O-N₁ covalent bond order (see Table 1). For Sc-Ni, the O-N₁ distances in the TS range between 1.21 and 1.28 Å, as compared to 1.18 Å in free N₂O. A substantially smaller O-N₁ bond order and longer O-N₁ distance (of 1.50

TABLE 2: Geometric Parameters (Distances in Å, Angles in Degrees) for the Transition Structure [Cu-N₂O][‡] at Various Levels of Theory and CCSD(T) Activation Barriers (kcal/mol) for These Different Structures

	M-O	O-N ₁	N ₁ -N ₂	N ₂ -N ₁ -O	E(CCSD(T)) (with ZPE)
MBPT2/TZVP	1.838	1.547	1.112	132.4	4.3
B3LYP/TZVP	1.854	1.499	1.141	125.4	3.4
CCSD/TZVP	1.899	1.469	1.157	121.2	4.0

Å) is found for the [Cu-O-N₁-N₂][‡] transition state. The M-O distances vary between 2.31 and 1.85 Å. This bond distance decreases substantially going from Mn to Cu (see Figure 2.B), coupled with an increasing M-O bond order. All these parameters clearly demonstrate that the character of the transition states is reagent-like but becomes more product-like when moving to the right in the 3d series, especially for Cu.

The quality of the B3LYP structures of the TS was checked by comparing with MBPT2 and CCSD structures. Because of the large computational effort required for a CCSD geometry optimization, only the structure of the TS of the Cu-N₂O reaction was checked. We expect that the transition states of the other metals will be calculated with a similar accuracy. The activation barrier of the three structures (B3LYP, MBPT2 and CCSD) was calculated at the CCSD(T) level for comparison. These structural parameters and activation barriers are shown in Table 2. One can see that the geometry and activation barrier of the B3LYP structure are in very good agreement with CCSD results. On the other hand, the MBPT2 structure is much more product-like than the CCSD structure. However, the activation barriers are all around 4 kcal/mol, lower than the experimental values of 9.5–10.9 kcal/mol.^{7,29}

3.2 Reaction Mechanism. An analysis of the B3LYP molecular orbitals revealed the important orbital interactions at the transition states, which are (for Ni) shown in Figure 3. In what follows, the d-orbitals will be denoted according to the xyz-orientation shown in Figure 1. The transition metal 3d- and 4s-orbitals interact mainly with the N₂O HOMO and LUMO. The N₂O HOMO is a π-orbital which is antibonding with respect to the O-N bond but bonding for the N-N bond. The LUMO is a π*-orbital with antibonding character for both the N-O and N-N bonds. At the transition state, a σ-interaction occurs between the metal 4s- and the in-plane N₂O LUMO, as shown in Figure 3A. As one can see, there is a strong bonding interaction on the oxygen side of N₂O, but also a weaker bonding interaction with N₂. The σ-interaction with the N₂O LUMO can lead to the delocalization of electrons from the filled 4s-orbitals on the metal into the empty N₂O LUMO. This back-donation results in a weakening of both the O-N₁ and N₁-N₂ bonds. Second, there are much weaker interactions between the metal 3d-orbitals and the N₂O HOMO, allowing a charge transfer in the opposite direction: electron donation from the N₂O HOMO to the metal. The metal 3d_{z²}-orbital stabilizes the in-plane N₂O HOMO through a σ-bond (as shown in Figure 3B). Finally, there is a very weak π-donation from the out-of-plane N₂O π-orbital into the metal 3d_{yz} orbital (Figure 3C).

B3LYP Mulliken and Bader charges on the atoms in the transition state structure indicate the importance of charge transfer along the 3d series. They are reported in Table 3, whereas Figure 4 shows the detailed pattern of the metal charges in the TS as a function of Z. Generally, Bader charges are considered to be more accurate than Mulliken charges, since the former are less basis set dependent. Our calculations show more ionic bonds with Bader compared to Mulliken population analysis. However, the two methods show the same trend along

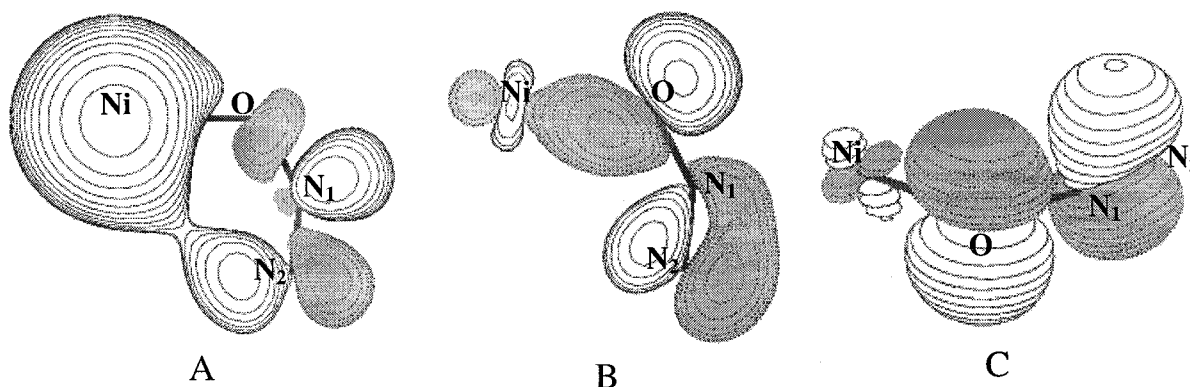


Figure 3. Bonding orbital interactions at the transition state structure $[\text{NiON}_1\text{N}_2]^\ddagger$: (A) σ -interaction between the Ni 4s and the N_2O in-plane LUMO; (B) σ -interaction between the Ni $3d_{z^2}$ and the N_2O in-plane HOMO; and (C) π -interaction between the Ni $3d_{yz}$ and the N_2O out-of-plane HOMO.

TABLE 3: Mulliken and Bader Charges and Spin Densities (between brackets) for Atoms in the $\text{M}-\text{O}-\text{N}_1-\text{N}_2$ Transition States, Obtained at the B3LYP/TZVP Level

	Mulliken		Bader			
	M	O	M	O	N_1	N_2
Sc($^2\text{A}''$)	-0.02 (-1.00)	0.14 (-0.94)	-0.53 (-0.01)	0.17 (-0.01)	0.21 (-0.04)	0.21 (-0.04)
Ti($^3\text{A}''$)	-0.08 (-1.99)	0.10 (-1.98)	-0.51 (-0.01)	0.19 (0.00)	0.23 (-0.01)	0.23 (-0.01)
V($^4\text{A}''$)	0.00 (-3.11)	0.21 (-3.13)	-0.52 (0.02)	0.17 (0.06)	0.13 (0.04)	0.13 (0.04)
Cr($^7\text{A}'$)	0.14 (-5.76)	0.27 (-5.62)	-0.53 (-0.07)	0.17 (-0.12)	0.07 (-0.18)	0.07 (-0.18)
Mn($^6\text{A}'$)	0.18 (-5.17)	0.37 (-5.15)	-0.55 (0.00)	0.17 (0.08)	0.00 (0.07)	0.00 (0.07)
Fe($^5\text{A}'$)	0.13 (-3.64)	0.33 (-3.98)	-0.55 (-0.02)	0.16 (0.00)	0.04 (0.00)	0.04 (0.00)
Co($^4\text{A}''$)	0.13 (-2.62)	0.31 (-2.59)	-0.53 (-0.03)	0.17 (-0.13)	0.06 (-0.24)	0.06 (-0.24)
Ni($^3\text{A}'$)	0.20 (-1.51)	0.42 (-1.44)	-0.55 (-0.05)	0.15 (-0.17)	-0.01 (-0.33)	-0.01 (-0.33)
Ni($^3\text{A}''$)	0.20 (-1.53)	0.40 (-1.45)	-0.55 (-0.05)	0.15 (-0.18)	-0.01 (-0.32)	-0.01 (-0.32)
Cu($^2\text{A}'$)	0.38 (-0.11)	0.56 (-0.11)	-0.58 (-0.31)	0.07 (-0.10)	-0.06 (-0.46)	-0.06 (-0.46)
free N_2O			-0.36 (0.00)	0.15 (0.00)	0.20 (0.00)	0.20 (0.00)

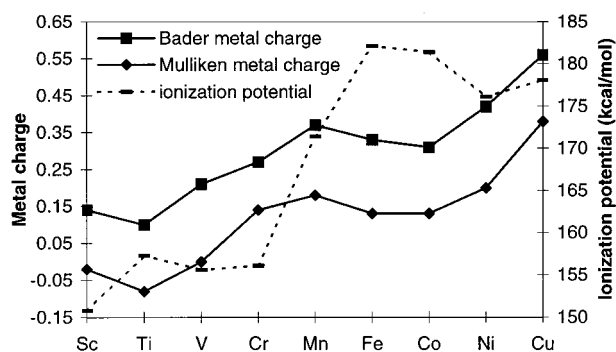


Figure 4. The metal charge (B3LYP/TZVP), Bader and Mulliken) in the TS and the ionization potential^{40,41} of the metal as a function of Z.

the 3d series: charge transfer from the metal to N_2O becomes more important when Z increases. This is in accordance with the increasing product-like character of the transition states with Z, as shown above. Almost no orbital interactions occur between Sc, Ti, V, and N_2O at the transition state, leading to very small metal charges. This very small electron transfer is in contradiction with the conclusion of Stirling,¹³ stating that electron transfer is an essential factor in the reaction mechanism of Sc-, Ti, V with N_2O .³⁰ However, the covalent character of the $\text{M}-\text{O}$ bond increases significantly when moving to the right through the 3d series. This is, as shown above, attended by a decrease of the $\text{M}-\text{O}$ distance, especially from Mn to Cu (see Figure 2.B). Charge transfer from the metal toward N_2O becomes then more important, due to the increasing metal $4s-\text{N}_2\text{O}$ LUMO back-donation. This back-donation clearly overrules the small donation from the N_2O HOMO to the metal. For Ni and Cu, a partial charge-transfer mechanism is indeed operative: the Bader

charges on the metal become 0.40 and 0.56, respectively. Bader charges on oxygen and nitrogen are also given in Table 3. As one can see, the charge donated by the metal is distributed mainly over oxygen and the terminal nitrogen.

It can be expected that the effect of charge transfer in the transition states is also reflected in the $\text{O}-\text{N}_1-\text{N}_2$ angles. The N_2O^- ion is bent, as opposed to the neutral linear N_2O molecule.³¹ The vertical electron affinity of N_2O is negative (-51.42 kcal/mol³²), which means that this process is highly unfavorable. The adiabatic process, on the other hand, is favorable, as shown by the experimental electron affinity of $+5.07$ kcal/mol.^{32,33} The course of the $\text{O}-\text{N}_1-\text{N}_2$ angle in the TS along the 3d series is represented in Figure 2.C and Table 1. Indeed, the pattern is conform with the trend in charge transfer. The transition states of Sc, Ti, and V exhibit $\text{O}-\text{N}_1-\text{N}_2$ angles around 170 degrees, in correspondence with the small amount of charge transfer for these metals. The $\text{O}-\text{N}_1-\text{N}_2$ angle generally decreases with the number of d-electrons, to a value of only 125 degrees for Cu, and even shows the same kink at Mn.

The B3LYP atomic spin densities for the TS are also shown in Table 3. For Sc–Co, the spin density is mainly concentrated on the metal atom, showing again the reagent-like character of these transition state structures and the small amount of charge transfer. In the case of Ni, B3LYP shows that a considerable amount of spin density (28% of the total spin) is also found on N_2O , due to the partial metal $4s-\text{N}_2\text{O}$ LUMO charge transfer. For Cu, however, 89% of the total spin is transferred from Cu to N_2O at the transition state.

Before the transition state is reached, the metal atom and N_2O form a very weak complex. The structural parameters of the energy minimum structures are shown in Table 4, with the exception of Sc because no stable Sc– N_2O complex was found.

TABLE 4: Geometric Parameters (Distances in Å, Angles in Degrees) for Energetic Minima M—O—N₁—N₂ Obtained at the B3LYP/TZVP Level

	M—O	O—N ₁	N ₁ —N ₂	M—O—N ₁	N ₂ —N ₁ —O
Ti(³ A'')	2.461	1.202	1.118	126.1	175.6
V(⁴ A'')	2.329	1.201	1.118	129.1	177.0
Cr(⁷ A')	2.472	1.194	1.120	108.0	178.4
Mn(⁵ A')	4.555	1.185	1.122	115.7	179.9
Fe(⁴ A)	3.836	1.185	1.122	144.2	179.8
Co(⁴ A'')	2.472	1.194	1.120	124.7	178.4
Ni(³ A')	2.383	1.195	1.120	122.1	177.9
Cu(² A')	3.271	1.186	1.122	117.8	179.5

The M—O distances are much longer in the encounter complex than those in the transition state structure, the M—O—N₁ angle is bent. The O—N₁—N₂ bond angle remains around 180 degrees (see Table 4), pointing to the absence of charge transfer in these encounter complexes. Indeed, the Bader charges on the metal (not reported here) remain close to zero in all cases.

As shown in Table 5, the M—N₂O binding energies calculated with DFT and CCSD(T) are all very low, varying around -1 kcal/mol. The Co—N₂O complex is not stable at the CCSD(T) level. As one can see from comparing column 1 and 2 in Table 5, the ZPE (zero-point vibrational energy) correction of the binding energy is always smaller than 0.5 kcal/mol.

The reaction coordinate at the region of the energy barrier is a linear combination of several internal coordinates: the M—O bond stretching, the O—N₁—N₂ bending and the M—O—N₁ bending. For the reactions with Sc—V, the O—N₁—N₂ bending seems the most important, whereas for Cr—Ni, the M—O stretching becomes more important. On the other hand, in the reaction with Cu the O—N₁ stretching is predominant at the region of the energy barrier.

3.3 Activation Barriers. In Table 5, we have also reported the activation barriers calculated at the B3LYP and CCSD(T) level. We report the values without and with ZPE correction. The ZPE correction reduces the activation energies. It is a small correction (0.7 kcal/mol) for Sc and increases when going to the right in the 3d series. At the CCSD(T) level, no ZPE could be calculated; therefore, the B3LYP ZPE's are used to correct the CCSD(T) activation barriers. We can now compare the B3LYP and CCSD(T) activation barriers to the experimental values in Table 5. For the atoms Sc, Ti, V, and Mn, the activation barriers are in reasonable agreement with experiment, both at the B3LYP and CCSD(T) level. We note that for the reaction of V and Ti with N₂O, the energy of the transition state is lower than that of the energy of the reagents. A barrier

is therefore only observed with respect to the energy of the M—N₂O complex. For Cr, Fe, Co, and Ni, the CCSD(T) activation barriers differ significantly from the B3LYP results. B3LYP tends to underestimate the activation barrier. On the other hand, with the exception of Cu and Ni, the CCSD(T) activation barriers are in close agreement with experiment.

The calculated activation energy for the reaction with Cu is somewhat smaller than the experimental estimate, both at the B3LYP and CCSD(T) level. We note that the CCSD(T) reference wave function also demonstrates the large charge transfer at the transition state of this reaction: an ion-pair transition state structure is calculated.

The Ni—N₂O reaction seems to be difficult to treat, not only theoretically but also experimentally. In the experimental studies of the Ni—N₂O reaction, it was found that the two lowest lying Ni states (4s²3d⁸ ³F₄) and 4s¹3d⁹ (³D₃) react with rate constants equal within experimental uncertainty.^{28,34} An Arrhenius fit of the measured rate constants was complicated due to a competing termolecular reaction. Assuming a negligibly small contribution of this reaction at 2.5 Torr, an activation barrier of 2.3 kcal/mol was estimated.²⁸ On the other hand, theoretically, the Ni atom is difficult to describe due to large correlation effects related to near-degeneracies. The Ni atom ground-state configuration is, without consideration of spin-orbit coupling, 4s¹3d⁹ (³D), with a 4s²3d⁸ (³F) state lying only 0.7 kcal/mol above the ground-state level.³⁵ CCSD(T), in combination with these basis sets, wrongly predicts a 4s²3d⁸ ground state, which is calculated 4 kcal/mol more stable than the 4s¹3d⁹ state. The 3d⁹4s¹ configuration is the most reactive, with a CCSD(T) activation barrier of 7.7 kcal/mol. The B3LYP results showed that the charge transfer from Ni 4s to N₂O π* was only partial. However, the charge transfer is estimated much larger in the CCSD(T) reference wave function, such that an ion-pair transition state structure (as for Cu) is calculated. The non-relativistic CCSD(T) activation barrier is slightly lower, i.e., 5.9 kcal/mol. The activation barrier on the 4s²3d⁸ surface is calculated to be significantly higher: 12.5 kcal/mol (estimated with regard to the energy of the 4s²3d⁸ Ni atom and N₂O).

The reaction of Cr with N₂O involves a change in spin, because the ground state of Cr is ⁷S₃, whereas CrO has a ⁵Π ground state. We did not attempt to find the point of intersection of the septet and quintet surfaces but report here only the transition state located on the septet surface. Because the transition states of the 3d M—N₂O reactions are all very reagent-like, it is reasonable to assume that the crossing between septet and quintet surfaces occurs after the transition state. An

TABLE 5: Binding Energies (B. E.) and Activation Barriers (E_b) at the B3LYP/TZVP and CCSD(T) Levels and Experiment^a (kcal/mol)

	B3LYP				CCSD(T)				experiment E _b
	B. E.		E _b		B. E.		E _b		
	no ZPE	with ZPE	no ZPE	with ZPE	no ZPE	with ZPE	no ZPE	with ZPE	
Sc(² A'')	/	/	1.9	1.2	/	/	0.0	-0.7	1.8 ^{4,8}
Ti(³ A'')	0.4	0.1	1.3	0.5	-2.9	-3.2	-1.2	-2.0	2.4 ^{4,8}
V(⁴ A'')	-1.5	-1.9	-1.2	-2.5	-1.1	-1.5	0.0	-1.3	2.4, ^{4,8} 2.2 ²⁸
Cr(⁷ A')	-0.2	-0.1	2.2	1.0	-1.2	-1.1	4.9	3.7	4.3; ⁴² 4.7 ²⁸
Mn(⁶ A')	0.0	0.0	9.0	7.8	-0.9	-0.9	10.5	9.3	10.1 ¹⁰
Fe(⁵ A')	-0.1	-0.0	6.7	5.3	-1.4	-1.5	11.3	9.9	10.1; ¹¹ 11.1 ³
Co(⁴ A'')	-0.4	-0.3	5.9	4.4	1.7	1.8	11.2	9.7	11.2 ²⁸
Ni(³ A')	-1.3	1.7	2.5	1.0	-1.4	-1.8	9.2	7.7	(2.7 ²⁸)
Ni(³ SA'')	/	/	3.7	2.2	/	/	14.0	12.5	/
Cu(² A')	-1.1	-1.1	6.8	4.3	-1.5	-1.5	5.9	3.4	9.5; ⁷ 10.9 ²⁹

^a For the B3LYP results, values with and without inclusion of the ZPE are shown. Activation barriers (E_b) calculated from the Arrhenius activation energy E_a with the formula E_b = E_a - nRT_{av}, with n = 0.5 and T_{av} = (T₁T₂)^{0.5}, where T₁ and T₂ are respectively the lowest and highest temperature of the measurements.⁸

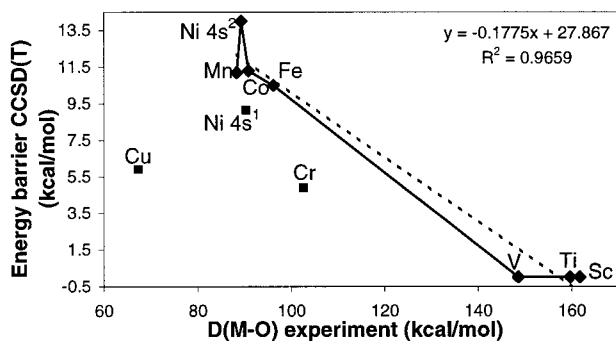


Figure 5. Correlation between dissociation energy (D) of $M-O^{36}$ (kcal/mol) and CCSD(T) activation barrier of the $M-N_2O$ reactions (kcal/mol).

activation barrier of 3.7 kcal/mol is then calculated, in good agreement with the experimental values (4.3 and 4.7 kcal/mol).

3.4 Reactivity along the 3d Series. The entire set of data of activation barriers of all the 3d transition metal atoms allows us to explore the trend in reactivity across the 3d series, and to check possible correlations between the activation barrier and various physicochemical parameters. According to the charge-transfer mechanism, a correlation between the activation barrier and the ionization potential of the transition metal atom could be expected. No such correlation was observed, using either the experimental or the CCSD(T) activation barriers. Along the same line, one would also expect that the charge transferred from the metal to N_2O increases when the ionization potential decreases. The course of the ionization potential of the transition metals along the 3d series is depicted in Figure 4, together with the metal charge at the TS. It is clear that there is no direct correlation between the metal charge in the TS and the ionization potential of the 3d transition metal. On the contrary, transition metal atoms with a low ionization potential (Sc, Ti, V, Cr) exhibit the lowest metal charges in the TS.

The semiempirical resonance model of Fontijn predicts that one should observe a correlation between the activation barrier and the sum of the ionization potential and $s-p$ promotion energy. Campbell already showed that there is no such correlation,^{10,11,28} and our results confirm Campbell's findings. The resonance interaction model can therefore not be expected to accurately predict the energy barriers for the 3d transition metals.

On the other hand, a reasonable correlation between the CCSD(T) activation barrier and the binding energy³⁶ of the formed metal oxide can be observed (as shown in Figure 5), at least for the transition metals with a $3d^n4s^2$ configuration. The binding energy of the transition metal oxide determines the exothermicity of the reaction. The most exothermic reactions thus proceed with the smallest energy barriers. Both experimental and theoretical studies have indicated that the binding energy of the first transition metal row oxides decreases (with a small deviation for Fe) as the atomic weight increases.^{36,37} The ScO , TiO , and VO bonds have triple bond character, with binding energies of more than 148 kcal/mol.^{36,37} The reactions of Sc, Ti, and V with N_2O are therefore very exotherm and proceed via very low energy barriers (below 2 kcal/mol). Much higher barriers are encountered for Mn–Co (around 9 kcal/mol), since the oxides of Mn–Co display only a double bond, resulting in smaller binding energies (between 88 and 96 kcal/mol,^{36,37}). The diminishing reagent-like character of the transition state structure going from Sc to Cu (as demonstrated in the previous section) is also in agreement with the decrease in exothermicity across the 3d series.

As can be seen from Figure 5, the activation barrier for reactions with atoms in a $3d^{n+1}4s^1$ configuration (Cr, Cu, and Ni $3d^9$) is much lower than predicted by the regression line. It has indeed been found that the $d^{n+1}s^1$ electron configuration is more reactive than the $d^n s^2$ configuration.^{6,12,38,39} The 4s orbital is much larger than 3d. Therefore, a diffuse closed s shell in the s^2 configuration causes electronic repulsive effects, reducing the reactivity.^{12,39}

4. Conclusions

In summary, the reactions of 3d transition metal atoms with N_2O have been studied using theoretical calculations. The transition state structures were determined and characterized at the DFT-B3LYP level. It was shown that the transition state structure becomes less reagent-like when moving to the right in the 3d row. For Sc–V, almost no charge transfer from the transition metal toward N_2O occurs at the transition state. On the other hand, charge-transfer becomes more important in the reactions with Cr–Cu, due to interaction between the metal 4s and the in-plane N_2O LUMO.

The activation barrier is reasonably well described at the CCSD(T) level, using the B3LYP structures. A good correlation between the activation barrier and the binding energy of the formed transition metal oxide was found: large binding energies result in a high exothermicity of the reaction and, apparently, a low energy barrier. As such, reactions with Sc, Ti, and V are characterized by the lowest activation barriers (below 2 kcal/mol). Atoms with a $3d^{n+1}4s^1$ configuration deviate from the trend. This configuration is much more reactive than $3d^n4s^2$.

Acknowledgment. This investigation has been supported by grants from the FlemishScience Foundation (FWO) and from the Concerted Research Action of the Flemish Government (GOA). We thank B. Joakim Persson for providing the basis sets for Cr, Mn, Fe, and Ni.

References and Notes

- (1) Wiesenfeld, J. R.; Yuen, M. *J. Chem. Phys. Lett.* **1976**, *42*, 293.
- (2) Ritter, D.; Weisshaar, J. C. *J. Phys. Chem.* **1989**, *93*, 1576.
- (3) Plane, J. M. C.; Rollason, R. J. *J. Chem. Soc., Faraday Trans.* **1996**, *92*, 4371.
- (4) Ritter, D.; Weisshaar, J. C. *J. Phys. Chem.* **1990**, *94*, 4907.
- (5) Campbell, M. L.; McClean, R. E. *J. Phys. Chem.* **1993**, *97*, 7942.
- (6) Campbell, M. L.; McClean, R. E. *J. Chem. Soc., Faraday Trans.* **1995**, *91*, 3787.
- (7) Narayan, S. A.; Futerko, P. M.; Fontijn, A. *J. Phys. Chem.* **1992**, *96*, 290.
- (8) Futerko, P. M.; Fontijn, A. *J. Chem. Phys.* **1991**, *95*, 8065.
- (9) Futerko, P. M.; Fontijn, A. *J. Chem. Phys.* **1993**, *98*, 7004.
- (10) Campbell, M. L. *J. Chem. Phys.* **1996**, *104*, 7515.
- (11) Campbell, M. L.; Metzger, J. R. *J. Chem. Phys. Lett.* **1996**, *253*, 158.
- (12) McClean, R. E.; Campbell, M. L.; Goodwin, R. H. *J. Phys. Chem.* **1996**, *100*, 751.
- (13) Stirling, A. *J. Phys. Chem. A* **1998**, *102*, 6565.
- (14) Kapteijn, F.; Rodriguez-Mirasol, J.; Moulijn, J. A. *Appl. Catal. B: Environ.* **1996**, *9*, 25.
- (15) Dandekar, A.; Vannice, M. A. *Appl. Catal. B: Environ.* **1999**, *22*, 179.
- (16) Perry, R. A.; Miller, J. A. *Int. J. of Chem. Kinet.* **1996**, *28*, 217.
- (17) Shelif, M.; Kummer, J. T. *Chem. Eng. Prog. Symp. Ser.* **1971**, *67*, 74.
- (18) Schäfer, A.; Huber, C.; Ahlrichs, R. *J. Chem. Phys.* **1994**, *100*, 5829.
- (19) Bader, R. F. W. *Atoms in Molecules, A Quantum Theory*. Clarendon Press: Oxford, 1990.
- (20) Bader, R. F. W.; Slee, T. S.; Cremer, D.; Kraka, E. *J. Am. Chem. Soc.* **1983**, *105*, 5061.
- (21) Frisch, M. J.; Trucks, G. W.; Schlegel, H. B.; Scuseria, G. E.; Robb, M. A.; Cheeseman, J. R.; Zakrzewski, V. G.; Montgomery, J. A., Jr.; Stratmann, R. E.; Burant, J. C.; Dapprich, S.; Millam, J. M.; Daniels, A. D.; Kudin, K. N.; Strain, M. C.; Farkas, O.; Tomasi, J.; Barone, V.; Cossi, M.; Cammi, R.; Mennucci, B.; Pomelli, C.; Adamo, C.; Clifford, S.;

Ochterski, J.; Petersson, G. A.; Ayala, P. Y.; Cui, Q.; Morokuma, K.; Malick, D. K.; Rabuck, A. D.; Raghavachari, K.; Foresman, J. B.; Cioslowski, J.; Ortiz, J. V.; Stefanov, B. B.; Liu, G.; Liashenko, A.; Piskorz, P.; Komaromi, I.; Gomperts, R.; Martin, R. L.; Fox, D. J.; Keith, T.; Al-Laham, M. A.; Peng, C. Y.; Nanayakkara, A.; Gonzalez, C.; Challacombe, M.; Gill, P. M. W.; Johnson, B. G.; Chen, W.; Wong, M. W.; Andres, J. L.; Head-Gordon, M.; Replogle, E. S.; Pople, J. A. *Gaussian 98*, revision A.5. Gaussian, Inc.: Pittsburgh, PA, 1998.

(22) Stanton, J. F.; Gauss, J.; Watts, J. D.; Nooijen, M.; Oliphant, N.; Perera, S. A.; Szalay, P. G.; Lauderdale, W. J.; Gwaltney, S. R.; Beck, S.; Balková, A.; Bernholdt, D. E.; Baeck, K.-K.; Rozyczko, P.; Sekino, H.; Hober, C.; Bartlett, R. J. *ACESII Version 3.0* Quantum Theory Project, University of Florida.

(23) Andersson, K.; Blomberg, M. R. A.; Fülscher, M. P.; Karlström, G.; Lindh, R.; Malmqvist, P.-Å.; Neogrády, P.; Olsen, J.; Roos, B. O.; Sadlej, A. J.; Schütz, M.; Seijo, L.; Serrano-Andrés, L.; Siegbahn, P. E. M.; Widmark, P.-O. *MOLCAS Version 4.0*. Department of Theor. Chem., Chem. Center, University of Lund, P. O. B. 124, S-221 00 Lund, Sweden, Lund, 1997.

(24) Pierloot, K.; Tsokos, E.; Roos, B. O. *Chem. Phys. Lett.* **1993**, *214*, 583.

(25) Pou-Amérgigo, R.; Merchán, M.; Nebot-Gil, I.; Widmark, P.-O.; Roos, B. O. *Theor. Chim. Acta* **1995**, *92*, 149.

(26) B. Joakim Persson and, P. Taylor, private communication.

(27) Widmark, P.-O.; Malmqvist, P.-Å.; Roos, B. O. *Theor. Chim. Acta* **1990**, *77*, 291.

(28) Campbell, M. L.; Kölsch, E. J.; Hooper, K. L. *J. Phys. Chem. A* **2000**, *104*, 11 147.

(29) Vinckier, K.; Verhaeghe, T.; Vanhees, I. J. *Chem. Soc., Faraday Trans.* **1994**, *90*, 2003.

(30) An inspection of the results of Stirling shows that the charge transfer becomes important only at N—O distances larger than 1.4 Å. The N—O distances in the transition states that we have calculated are much smaller than that. The charge transfer observed by Stirling thus occurs mainly after the transition state.

(31) McCarthy, M. C.; Allington, J. W. R.; Sullivan, K. O. *Mol. Phys.* **1999**, *96*, 1735.

(32) Hopper, D. G.; Wahl, A. C.; Wu, R. L. C.; Tiernan, T. O. *J. Chem. Phys.* **1976**, *65*, 5474.

(33) Tiernan, T. O.; Wu, R. L. C. *Adv. Mass Spectrom.* **1978**, *7A*, 136.

(34) Matsui, R.; Senba, K.; Homma, K. *J. Phys. Chem. A* **1997**, *101*, 179.

(35) Andersson, K.; Roos, B. O. *Chem. Phys. Lett.* **1992**, *191*, 507.

(36) Merer, A. J. *Annu. Rev. Phys. Chem.* **1989**, *40*, 407.

(37) Bauschlicher, C. W.; Maitre, P. *Theor. Chim. Acta* **1995**, *90*, 189.

(38) Brown, C. E.; Mitchell, S. A.; Hackett, P. A. *J. Phys. Chem.* **1991**, *95*, 1062.

(39) Ritter, D.; Carroll, J. J.; Weisshaar, J. C. *J. Phys. Chem.* **1992**, *96*, 10 636.

(40) Moore, C. E. *Atomic Energy Levels, as Derived from the Analyses of Optical Spectra, Vol. I*; U.S. Government Printing Office, Washington 25, D. C., 1949.

(41) Moore, C. E. *Atomic Energy Levels, as Derived from the Analyses of Optical Spectra, Vol. II*; U.S. Government Printing Office, Washington 25, D. C., 1952.

(42) Fontijn, A.; Blue, A. S.; Narayan, A. S.; Bajaj, P. N. *Combust. Sci. and Technol.* **1994**, *101*, 59.